Flexible Nanocellulose/Poly(ethylene glycol) Diacrylate Hydrogels with Tunable Poisson's Ratios by Masking and Photocuring

Chanyu Bai,[a] Aimin Tang,[a,*] Shan Zhao,[a] and Wangyu Liu [b]

Flexible hydrogels with an adjustable Poisson's ratio were prepared, offering a way to simulate the behavior of natural organisms, expressing corresponding deformation in response to external forces. Nanofibrillated cellulose (NFC) particles were blended with photo-curable resin poly(ethylene glycol) diacrylate (PEGDA), and flexible NFC/PEGDA hydrogels with positive, near zero, and negative Poisson's ratios (0.66 ± 0.31, 0.17 ± 0.28, and -0.39 ± 0.26, respectively) and were successfully prepared using masking and photocuring. Furthermore, the effects of different curing times and mask apertures were investigated. The clarity and structural precision of the hydrogels were used to evaluate the effects of the preparation procedures. A curing time of 20 s and a mask aperture of 5 mm were the ideal conditions for preparation of NFC/PEGDA hydrogels. Further, addition of NFC resulted in excellent hydrogel flexibility and enhanced mechanical properties. The fabrication of NFC/PEGDA hydrogels with high structural precision and tunable Poisson's ratios has the potential for application in wearable devices and intelligent monitoring equipment.

Keywords: Nanocellulose; Hydrogel; Poisson's ratio

Contact information: a: State Key Laboratory of Pulp and Paper Engineering, South China University of Technology, Guangzhou 510640, PR China; b: School of Mechanical and Automotive Engineering, South China University of Technology, Guangzhou 510640, PR China;
** Corresponding author: amtang@scut.edu.cn*

INTRODUCTION

Cellulose is the oldest, most abundant polymer of natural origin on the earth. It is a biodegradable and renewable biomass resource with a wide range of sources. After decades of relevant research, nanocellulose was successfully prepared from cellulose. Nanocellulose is the main raw material used to prepare flexible hydrogels due to its high surface area, high elasticity, biocompatibility, low-toxicity, and degradability.

Hydrogels are a family of three-dimensional hydrophilic polymeric network materials with a high water content that have excellent mechanical properties, good biocompatibility and biomimetic characteristics, and have been extensively applied in wearable sensors (Liu *et al.* 2017; Lim *et al*. 2019; Zheng *et al.* 2019). Recently, a new strain sensor made of GN-CNF@PVA hydrogel was reported, which can effectively identify and monitor human movement behavior (Zheng *et al.* 2019). Further, a wearable soft strain sensor built using conductive, elastic, self-healing, and strain-sensitive hydrogels was created that can effectively monitor finger joint motions (Liu *et al.* 2017).

Natural tissues have complex structures, and different parts of human tissue have different Poisson's ratios. For instance, the Poisson's ratios of biological tissues, such as cartilage, ligaments, and meniscus, are about zero (Jurvelin *et al.* 2000; Abdelgaied *et al.*

2015; Danso *et al.* 2018; Men *et al.* 2018). Furthermore, the Poisson's ratio and the Young's modulus of cancerous skin are 0.43 ± 0.12 and 52 KPa, respectively (Tilleman *et al.* 2004). Combining these structural characteristics with biocompatible hydrogels to simulate natural tissue behaviour and design, an *in vitro* and *in vivo* diagnostic tool has great potential for development (Tilleman *et al.* 2004). Therefore, simulating the structural and mechanical behaviour of these natural tissues and designing and manufacturing materials with different Poisson's ratios for flexible wearable devices and intelligent monitoring are important research areas that have practical value.

However, hydrogels that have a special Poisson's ratio tend to have special geometries and complex shapes that are difficult to prepare by conventional 3D printing methods (Fozdar *et al.* 2011; Soman *et al.* 2012). For example, micro-extrusion 3D printing has defects, such as low manufacturing speed, resolution dependent on nozzle specifications, and poor forming effects (Leppiniemi *et al.* 2017; Li *et al.* 2017; Nguyen *et al.* 2017; Cheng *et al.* 2019). Low forming precision may dramatically alter the Poisson's ratio (Huang *et al.* 2018). As cellulose is non-thermoplastic, nanocellulose cannot be utilized in fused deposition modelling (FDM), which has limited the application of nanocellulose in 3D printing. In contrast with conventional 3D printing methods, masking and photocuring technology is a nozzleless technology with which printing time is independent of complexity (Wang *et al.* 2015; Mandrycky *et al.* 2016). Further, masking and photocuring technology offers high precision and cell viability, making it the most promising 3D printing technology currently applicable. Poly(ethylene glycol) diacrylate (PEGDA) is a non-toxic, photo-curable resin with reliable biodegradability that is often used as a 3D printing material (Cha *et al.* 2014; Hribar *et al.* 2014; Stahl *et al.* 2014). Adding PEGDA renders nanofibrillated cellulose (NFC) photocurable. The authors' previous studies have provided a theoretical basis for the successful preparation of NFC/PEGDA hydrogels (Tang *et al.* 2018, 2019).

In this study, flexible NFC/PEGDA hydrogels with three typical Poisson's ratios were successfully fabricated *via* photocuring with a photographic mask. Because curing time and optimal mask aperture may affect the forming precision of hydrogels during masking and photocuring fabrication, the influence of curing time on the clarity and precision of NFC/PEGDA hydrogels was investigated. Then, the optimal curing time was used to prepare honeycomb hydrogels of different sizes. The purpose was to identify the optimal mask aperture to achieve the highest possible precision. Finally, the effects of NFC addition on the mechanical properties and Poisson's ratios of the hydrogels were investigated. This study aimed to achieve rapid prototyping of flexible NFC/PEGDA hydrogels *via* masking and photocuring technology and provide a theoretical basis for studying the application of NFC-based hydrogel materials in wearable devices and intelligent monitoring.

EXPERIMENTAL

Materials

The 2, 2, 6, 6- tetramethylpiperidine -1- oxyl (TEMPO, free-radical quencher) was obtained from Tianjin Chemical Co., Ltd. (Tianjin, China). The NaClO with a concentration of 10% was obtained from Tianjin Fuyu Fine Chemicals Co., Ltd. (Tianjin, China). Both NaBr and KBr were obtained from Tianjin Kermel Chemical Reagent Co., Ltd. (Tianjin, China), and poly(ethylene glycol) diacrylate (PEGDA, M_n = 700) was

purchased from Sigma-Aldrich (Shanghai, China). Irgacure 2959 was obtained from Ciba Specialty Chemicals (Basel, Switzerland) and used to initiate monomer crosslinking.

Methods

Preparation of NFC/PEGDA UV-curing mixture

The oxidation of cellulose was carried out with bleached sulphate eucalyptus pulp *via* TEMPO/NaBr/NaClO alkaline medium oxidation system according to the methods of Saito and Nishiyama (2007). The bleached eucalyptus kraft pulp (20 g) was suspended in water with the addition of TEMPO (0.01 M, 0.1 mmol/g) and sodium bromide (0.4 M, 1 mmol/g). A 9 mmol/g NaClO (effective chlorometer) solution was added to adjust the pH to 10, and the concentration of the whole oxidation system was 2%. The pH was kept at 10 *via* addition of 0.1 M and 0.5 M NaOH using a pH stat until the final pH (10 + 0.02) was stable. Then, anhydrous ethanol was used to terminate the reaction. The TEMPO-oxidized cellulose was washed repeatedly with deionized water through filtration until no Cl^- was detected. The material was then stored at 4 °C. The carboxylate content of the TEMPO-oxidized cellulose was determined with an electrical conductivity titration method. The nanofibrillated cellulose particles (NFC) were obtained by ultrasonic treatment (NP; Guangzhou Newpower Ultrasonic Electronic Equipment Co., Ltd., Guangzhou, China) of oxidized cellulose with content of 2% for 90 min, the carboxylate content of oxidized cellulose was 1.74 mmol/g.

A 25 g quantity of the photo-cured resin PEGDA was added into three 75 g NFC water suspensions with different mass ratios (0 wt%, 0.75 wt%, and 1.5 wt%). A 0.1 wt% photo-initiator (I-2959; Sigma-Aldrich (Shanghai) Trading Co., Ltd., Shanghai, China) was added to each group, and the NFC/PEGDA mixtures were then placed in a water bath at 35 °C and magnetically stirred for 20 min. The formula of the resultant NFCs/PEGDA UV-curing mixtures is provided in Table 1.

Table 1. The Formulae of NFC/PEGDA UV-curing Mixtures

Sample	PEGDA (g)	NFC Suspensions	Deionized Water (g)	Mixture PEGDA Content (wt%)	Mixture NFC Content (wt%)
B-1	25	0	75	25	0
B-2	25	75 g, NFC content 1%	0	25	0.75
B-3	25	75 g, NFC content 2%	0	25	1.5

Fabrication of UV-cured NFC/PEGDA hydrogels

Images of three typical Poisson's ratio structures (honeycomb, reversed semi-re-entrant (RSRE) and auxetic structures), and the honeycomb structure with different apertures were designed by computer-aided drafting (CAD) software (AutoCAD, Autodesk Company, AutoCAD 2013, San Rafael, CA, USA). After optical printing, they were made into a mask film to control the geometrical structure of the hydrogel. The photo-cured mixture was injected into the mold (55 mm × 25 mm × 1 mm), above which was placed the mask film used to shape the solid portion. Then, the mold and the mask film were placed on an opaque bottom plate and put into a UV curing rapid prototyping machine (Shenzhen Huihongyu Technology Co., Ltd., Shenzhen, China). Finally, the UV-curing NFC/PEGDA hydrogels with different geometrical structures and apertures were constructed after a certain period of curing. The prepared samples were rinsed with

deionized water and stored at 4 °C for subsequent use. The preparation routine of hydrogels obtained from the PEGDA and NFC using masking and photocuring is shown in Fig. 1.

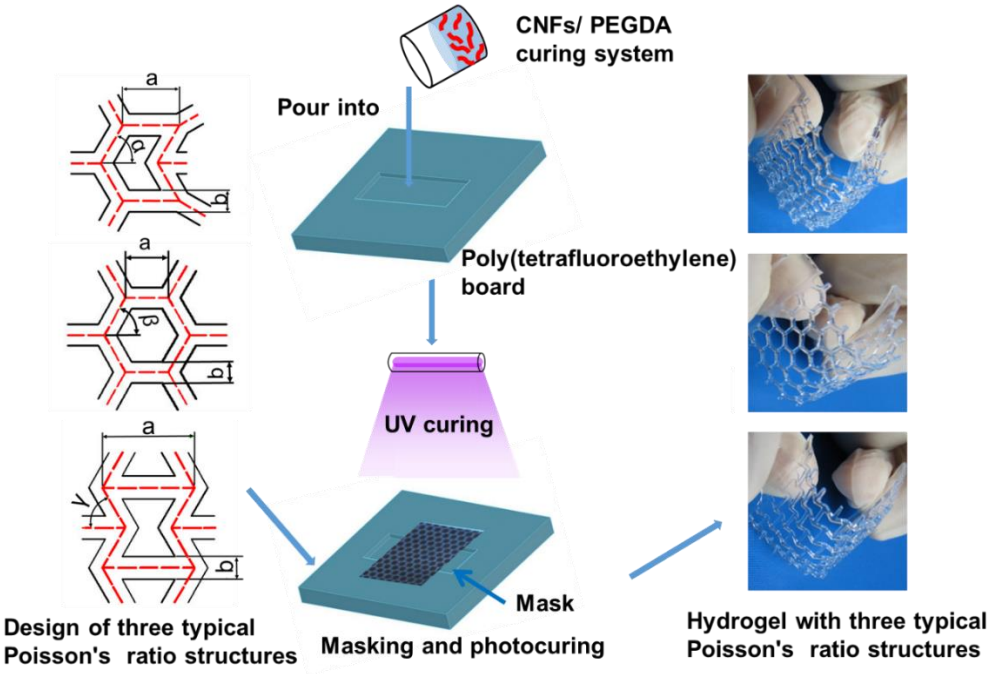

Fig. 1. Schematic representation of the masking and photocuring approach used to construct NFC/PEGDA hydrogels with a tunable Poisson's ratio

Assessing the clarity and the precision of hydrogels

A digital camera (EOS M50; Canon Corporation, Tokyo, Japan) and optical microscope (OLYMPUS BX51; Olympus Corporation, Shinjuku, Tokyo) were used to assess clarity and precision by observing the appearance and structural outlines of the NFC/PEGDA hydrogels. At the same time, the cross-sectional structures of three honeycomb structures were fitted with MATLAB (MathWorks, Matlab2013a, Natick, MA, USA) to verify the forming precision of NFC/PEGDA hydrogels.

Strain testing

Strain tests were conducted to analyze the mechanical properties and determine the Poisson's ratio of the NFC/PEGDA hydrogels. The prepared NFC/PEGDA hydrogel specimens, with a dumbbell structure, were loaded into a universal testing machine (Instron-5565; Instron Corporation, Canton, MA, USA) by attaching one side to an immobile platform and attaching the other side to a mobile platform. The experiments were conducted with a 100 N sensor at a crosshead displacement rate of 0.5 mm/min (three replicates).

Calculation of Poisson's ratios

The Poisson's ratios of the honeycomb samples were obtained *via* an image-based measurement during tensile testing by calculating the ratio of transverse to longitudinal strain (Wang *et al.* 2014). The movement of the marked point in the gel structure was recorded by a camera during the tensile process, and each sample was measured three times.

RESULTS AND DISCUSSION

Structural Design and Mask Film Fabrication

The images of three typical Poisson's ratio lattice structures are shown in Fig. 2A. Each mask had a specific unit grid arranged along the XY-axis that was designed by AutoCAD. Figure 2B shows the mask films with three different Poisson's ratio lattice structures and different apertures of the honeycomb structure fabricated by optical printing. The masks determined the shape of the fabricated microstructure (Sun *et al.* 2005). The opaque area was filled-in black, and the illuminated area was solidified instantly through one exposure. The dark regions remained liquid during the curing process. For each of the three kinds of different mask structures, the thickness of the wall (illuminated area) was 0.5 mm. The aperture of the masks c, d, and e with a honeycomb structure were 5 mm, 2.5 mm, and 0.5 mm, respectively. The wall thicknesses for these masks c, d, and e were 0.5 mm, 0.25 mm, and 0.1 mm, respectively.

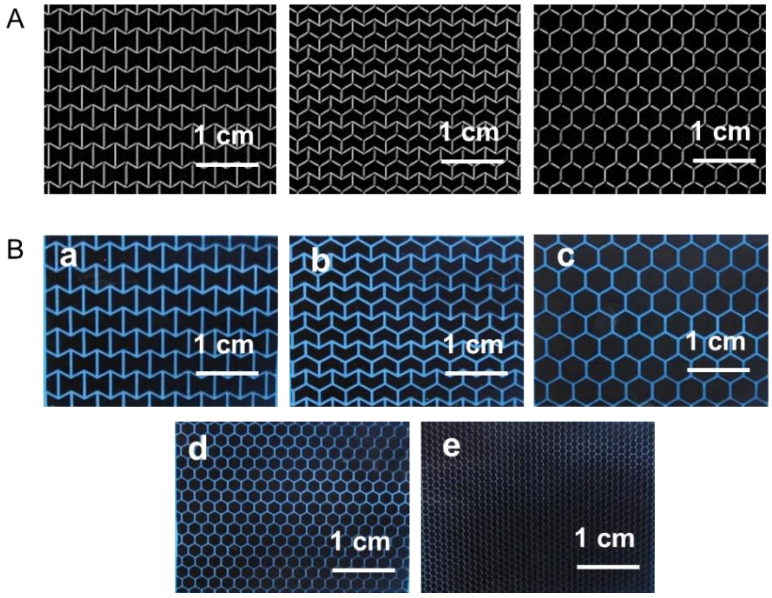

Fig. 2. (A) AutoCAD images of different Poisson's ratios; (B) Mask films with different Poisson's ratios and apertures (a is an auxetic structure, b is an RSRE structure, c is honeycomb (I), d is honeycomb (II), and e is honeycomb (III))

Poisson's Ratio of NFC/PEGDA Hydrogels

The masking and photocuring technology based on the application of a masking film was used to fabricate NFC/PEGDA hydrogels with three particular Poisson's ratios (Fig. 3). The digital photos of the 3D hydrogels constructed from the curing mixture (1.5 wt% NFC, 25 wt% PEGDA) and cured for 20 s using masks with different grid structures and an aperture of 5 mm are shown in Fig. 3A. The results indicated that NFC/PEGDA hydrogels with a honeycomb structure, an RSRE structure, and an expanded structure were all uniform and clear, and the structures matched the mask. The hydrogels did not exhibit any fractures and maintained good structural integrity and flexibility under flexure up to 180°, suggesting that the tunable Poisson's ratio of 3D materials could be achieved with masking and photocuring.

Figure 3B shows the Poisson's ratio of NFC/PEGDA hydrogels with a honeycomb structure, an RSRE structure, and an auxetic structure. The Poisson's ratio of the hydrogel

was analyzed by calculating the ratio of transverse strain to longitudinal strain of the hydrogel. The theoretical Poisson's ratio of the honeycomb structure, RSRE structure, and expanded structure are 0.8 ± 0.3, 0 ± 0.3, and -0.8 ± 0.3, respectively. Figure 3B shows that the experimental Poisson's ratios of NFC/PEGDA hydrogels with a honeycomb structure, an RSRE structure, and an auxetic structure were 0.66 ± 0.31, 0.17 ± 0.28, and -0.39 ± 0.26, respectively, which demonstrated that the different structures had different Poisson's ratios. This indicated that the NFC/PEGDA hydrogels were within the range of the Poisson's ratios of these three special structures. Therefore, the NFC/PEGDA UV-curing system could be used to prepare hydrogel materials with a particular Poisson's ratio.

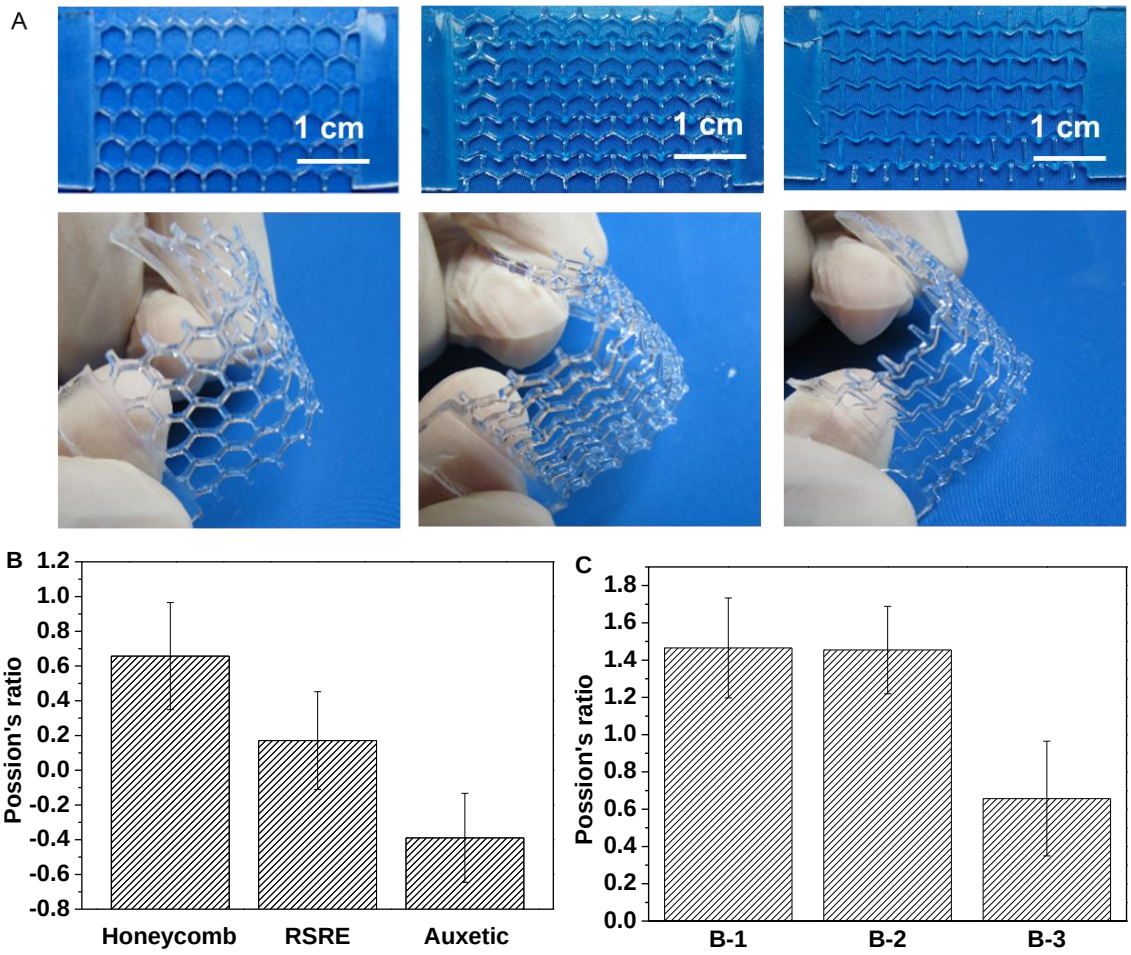

Fig. 3. (A) Digital photos of NFC/PEGDA hydrogels with different Poisson's ratios; UV-curing mixture: 1.5 wt% NFCs, 25 wt% PEGDA; (B) Poisson's ratios of NFC/PEGDA hydrogels with different geometric constructions; (C) Poisson's ratios of NFC/PEGDA hydrogels with honeycomb structures with different NFC contents

To determine if adding NFC would change the Poisson's ratio of NFC/PEGDA hydrogels, pure PEGDA hydrogel and NFC/PEGDA hydrogels with NFC contents of 0.75 wt% and 1.5 wt% were studied (Fig. 3C). The Poisson's ratios of the B-1, B-2, and B-3 structures were 1.47 ± 0.27, 1.45 ± 0.23, and 0.66 ± 0.31, respectively. Poisson's ratio decreased as the content of NFC increased. Even so, all three samples have positive Poisson's ratio, which is related to the fact that they all have the same honeycomb structure.

Clarity Analysis

To find the appropriate masking and photocuring printing process for the NFC/PEGDA hydrogels, a digital camera and optical microscope were used to analyze the clarity and precision by observing the appearance and structural outlines of the NFC/PEGDA hydrogels. First, the influence of curing time on the clarity of the NFC/PEGDA hydrogels made from the photo-curing mixture (1.5 wt% NFC and 25 wt% PEGDA) was studied. The digital photographs of the NFC/PEGDA hydrogels with different photo-curing times are shown in Fig. 4. The honeycomb hydrogels exhibited uniform and complete shape and excellent flexibility at all curing times. Apertures and the thickness between the pores of the hydrogels after different curing times are listed in Table 2. Figure 4 and Table 2 show that the honeycomb hydrogel with an aperture of 4.38 mm and a thickness of 0.52 mm was much thinner with a curing time of 15 s than with curing times of 20 s or 25 s. This was likely because the PEGDA group in the NFC/PEGDA UV-curing system was not fully crosslinked due to the short curing time. With a curing time of 25 s, the aperture of honeycomb hydrogel decreased to 3.81 mm, which is smaller than the mask aperture size. A long curing time can result in excessive crosslinking of the PEGDA component in the NFC/PEGDA, leading to solidification of the edge of the illuminated area. However, with a curing time of 20 s, the honeycomb hydrogel microstructures exhibited clear outlines and the aperture size (4.42 mm) and mask aperture size (5 mm) were similar. Thus, to obtain a clearer outline, the photo-curing time should be 20 s.

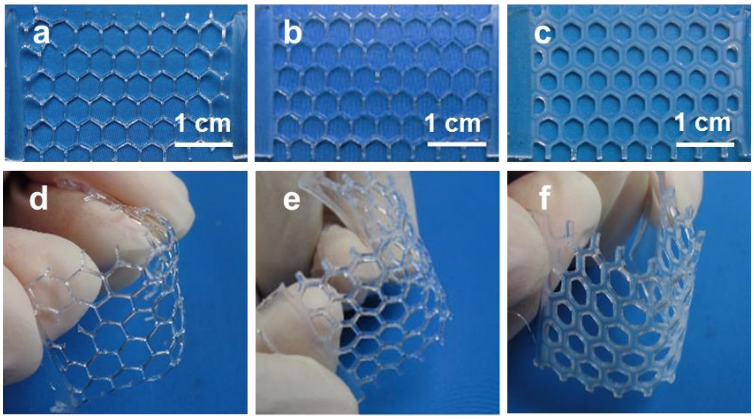

Fig. 4. Digital photos of NFC/PEGDA hydrogels with different photo-curing times; photo-curing mixture: 1.5 wt% NFC and 25 wt% PEGDA; (a) and (d): samples photo-cured for 15 s; (b) and (e): samples photo-cured for 20 s; (c) and (f): samples photo-cured for 25 s

Table 2. Geometric Parameters of Honeycomb Pores after Different Photo-curing Times

Sample	Curing Time (s)	Aperture (mm)	Thickness (mm)
a	15	4.38	0.52
b	20	4.42	0.82
c	25	3.81	1.39

The aperture of the mask was 5 mm and the thickness between the pores was 0.5 mm

Analysis of the Precision

The effect of aperture on the printing precision of NFC/PEGDA hydrogels was studied. The digital photo and hydrogel aperture measurement results of the NFC/PEGDA hydrogels with various apertures obtained from the photo-curing mixture (1.5 wt% NFC, 25 wt% PEGDA) and cured for 20 s are shown in Fig. 5 and Table 3. The apertures of the masks used of the honeycombs (I), (II), and (III) were 5 mm, 2.5 mm, and 0.5 mm, respectively. The digital images in Fig. 5A show the different apertures of the NFC/PEGDA hydrogels. Figure 5A shows that the hydrogel with the honeycomb (I) structure was complete and uniform with no obvious damage, whereas the uniformity of the hydrogel with the honeycomb (II) structure was worse and had a relatively obscure outline. The hydrogel with the honeycomb (III) structure was damaged, but it had excellent flexibility. The three average aperture values of the prepared honeycombs (I), (II), and (III) were 4.55 mm, 1.83 mm, and 0.62 mm, respectively. The relative errors of the mask aperture were 9.00%, 26.80%, and 24.00%, respectively (Table 3). Hydrogel clarity increased as honeycomb mask size increased, which may have been due to the light source. When the aperture is small, the light source is non-uniform, leading to unclear structural contours.

Based on these results, the influence of the aperture on the precision of the NFC/PEGDA hydrogels was explored by magnifying the crossed edges of the regular hexagons of honeycomb (I), honeycomb (II), and honeycomb (III) (Fig. 5B). The crossed edges of the regular hexagons of honeycomb (I) were nearly hexagonal at 120°, and the hexagonal edges were smooth without any obvious depression and uplift. With an aperture mask of 2.5 mm, the angles of the honeycombs (II) were rounder and the hexagonal edges had uneven regions. When the aperture of the mask decreased to 0.5 mm, the angles of honeycomb (III) became almost rounded. It can be seen that the NFC/PEGDA curing system can be used to prepare NFC/PEGDA hydrogel with controllable geometry and size.

The angle changes at the intersection points of the hexagons in the honeycomb structures were further confirmed by the curvature radius curve formed using MATLAB™, which used a least squares fitting contour curve and combined curvature information to extract feature-points (shown in Fig. 5B). Figure 5B shows the fitting curves of the three kinds of honeycomb structure in cross-section, where honeycomb (I), honeycomb (II), and honeycomb (III) were fitted by Y_1, Y_2, and Y_3, respectively, as follows:

$$Y_1 = 5.064 \times 10^{-8}X^5 - 2.711 \times 10^{-5}X^4 + 0.005598X^3 - 0.5473X^2 + 24.80X - 289.8 \quad (1)$$

$$Y_2 = 3.234 \times 10^{-9}X^5 - 2.490 \times 10^{-6}X^4 + 0.0007032X^3 - 0.08021X^2 + 1.451X + 404.5 \quad (2)$$

$$Y_3 = -1.399 \times 10^{-10}X^5 + 1.559 \times 10^{-6}X^4 - 0.0005480X^3 + 0.07327X^2 - 4.497X + 269.2 \quad (3)$$

The angle change of the fitting curve was consistent with that of a hexagon, which shows the printing accuracy of the hydrogel. The results indicated that the contour deterioration in three-dimensional hydrogel was caused by non-uniform ultraviolet light with decreasing mask aperture, resulting in high-demand control of the masking and photocuring process (UV light intensity, UV light path). Consequently, the minimum aperture of the NFC/PEGDA hydrogel was 5 mm due to the precision of the chosen method.

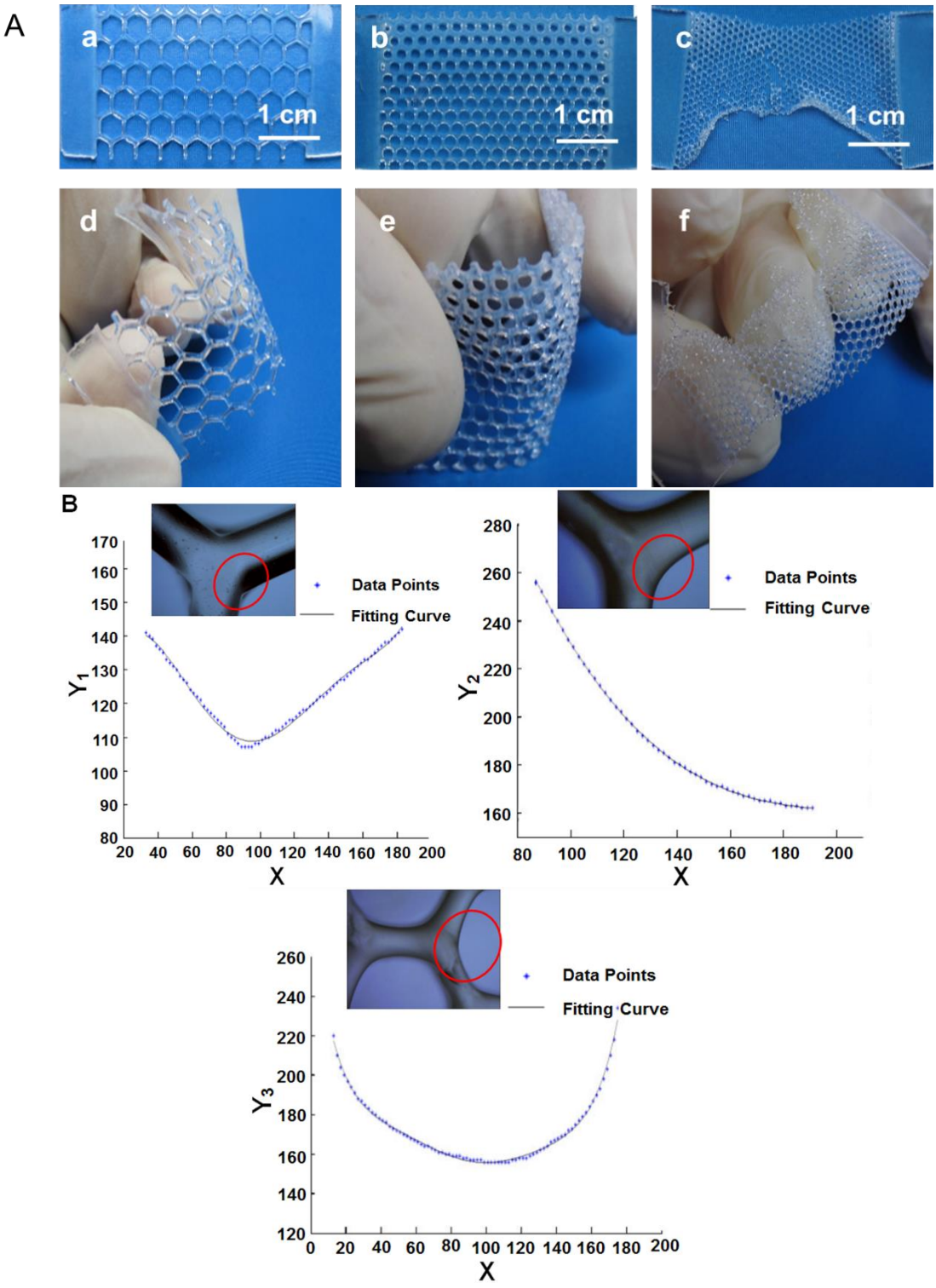

Fig. 5. (A) Digital photographs of NFC/PEGDA hydrogels with different structure sizes; (B) Optical microscope photographs of hydrogels with different structure sizes and their corresponding edge fitting curves (the edge fitting curves of the three honeycomb structures I, II, and III were Y_1, Y_2, and Y_3, respectively); Photo-curing mixture: 1.5 wt% NFC and 25 wt% PEGDA; photo-curing time, 20 s ((a) and (d): honeycomb (I) samples with a mask aperture of 5 mm; (b) and (e): honeycomb (II) samples with an aperture of 2.5 mm; (c) and (f): honeycomb (III) samples with an aperture of 0.5 mm

Table 3. The Geometric Parameters of the Honeycomb Structures

Sample	Mask Aperture (mm)	Hydrogel Aperture (mm)	Relative Error (%)
I	5.00	4.55	9.00
II	2.50	1.83	26.80
III	0.50	0.62	24.00

Mechanical Properties of NFC/PEGDA Hydrogels

The NFC hydrogels are highly hydrated porous cellulosic soft materials with good mechanical properties. To explore the influence of NFC on the mechanical properties of the NFC/PEGDA hydrogels, pure PEGDA hydrogels and NFC/PEGDA hydrogels with NFC contents of 0.75 wt% and 1.5 wt% were prepared. The tensile properties of the NFC/PEGDA hydrogels were measured *via* universal tensile testing machine. Figure 6A shows the stress-strain diagrams of the pure PEGDA hydrogel (B-1) and the NFC/PEGDA hydrogels with different NFC contents (B-2: 0.75 wt% NFC; B-3: 1.5 wt% NFC). The maximum stresses were 0.025 MPa, 0.065 MPa, and 0.064 MPa, respectively. The maximum strains were 0.015 mm/mm, 0.049 mm/mm, and 0.051 mm/mm, respectively. The addition of NFC noticeably improved the mechanical performance of the hydrogels as the maximum tensile stress increased from 0.025 MPa to 0.065 MPa and the maximum strain increased from 0.015 mm/mm to 0.051 mm/mm. The stress-strain curve formed by the X-axis envelope reflects the material's absorption of strain energy and its toughness. Comparing the envelope area under the stress-strain curves of the B-1, B-2, and B-3 NFC/PEGDA hydrogels shows that B-2 and B-3 have much greater toughness than B-1, indicating that the addition of NFC noticeably increased the toughness of the NFC/PEGDA hydrogel material. This flexibility is conducive to the application of hydrogels in flexible wearable devices.

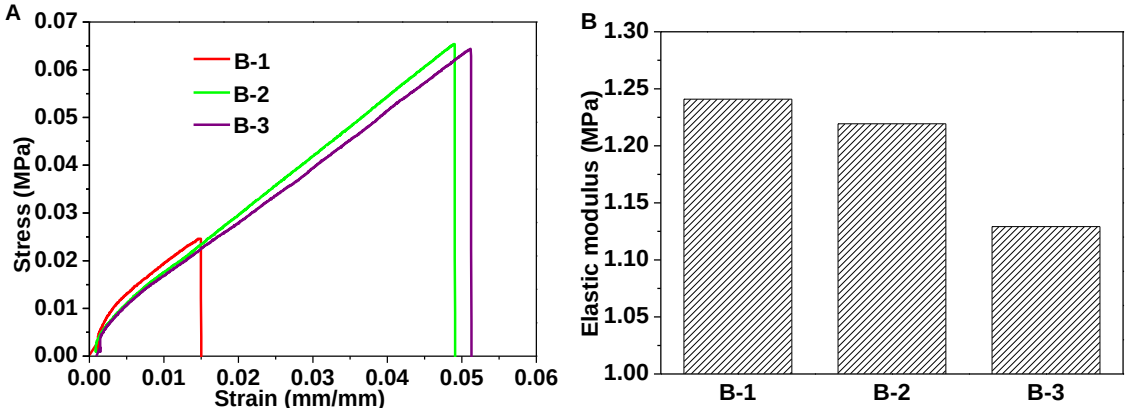

Fig. 6. Stress-strain curves (A) and elastic modulus (B) of NFC/PEGDA hydrogels with different NFC contents; B-1: pure PEGDA; B-2: 0.75 wt% NFC; B-3: 1.5 wt% NFC with a 20 s photo-curing time

The elastic modulus reflects the difficulty in elastically deforming a material. To confirm how the NFC contribute to the toughness of NFC/PEGDA hydrogel, the elastic modulus of the NFC/PEGDA hydrogels with different NFC contents are shown in Fig. 6B.

The elastic moduli of B-1, B-2, and B-3 were 1.24 MPa, 1.22 MPa, and 1.13 MPa, respectively.

With an increased amount of NFC, the elastic modulus of the NFC/PEGDA hydrogels decreased slightly and the rigidity decreased accordingly. Then, the elastic deformation in the hydrogel material at a given stress increased, which was consistent with the stress-strain results.

CONCLUSIONS

1. In this study, by manipulating the processing parameters of masking and photocuring technology, hydrogels with good precision, controllability, and utility were successfully prepared. A class of 3D NFC/PEGDA hydrogels with particular Poisson's ratios (the experimental Poisson's ratios of hydrogels with a honeycomb structure, an RSRE structure, and an auxetic structure were 0.66 ± 0.31, 0.17 ± 0.28, and -0.39 ± 0.26, respectively) were fabricated.
2. With a curing time of 20 s, the honeycomb hydrogels exhibited a uniform, complete shape and excellent flexibility.
3. The relative error of the aperture between the hydrogel and the designed mask was only 9.00% when the mask aperture was 5 mm.
4. The optimal NFC/PEGDA hydrogel with a 1.5 wt% NFC content had a tensile stress and strain that were approximately 2.6 times and 3.4 times higher than that of the pure PEGDA hydrogel. The NFC/PEGDA hydrogels have much greater toughness than pure PEGDA hydrogel.
5. The preparation of hydrogels with simulated natural tissue behavior, good biocompatibility, and low toxicity provides a potential research avenue for flexible wearable devices and intelligent monitoring.

ACKNOWLEDGMENTS

This research was supported by the National Natural Science Foundation of China (Grant No. 51875214) and the National Natural Science Foundation of China (No. 11972161).

REFERENCES CITED

Abdelgaied, A., Stanley, M., Galfe, M., Berry, H., Ingham, E., and Fisher, J. (2015). "Comparison of the biomechanical tensile and compressive properties of decellularised and natural porcine meniscus," *J. Biomech.* 48(8), 1389-1396. DOI: 10.1016/j.jbiomech.2015.02.044

Cha, C., Soman, P., Zhu, W., Nikkhah, M., Camci-Unal, G., Chen, S., and Khademhosseini, A. (2014). "Structural reinforcement of cell-laden hydrogels with microfabricated three dimensional scaffolds," *Biomater. Sci.* 2(5), 703-709. DOI: 10.1039/C3BM60210A

Cheng, F., Zhou, J. P., Xu, X. D., Jiang, Y. N., Shi, H. C., and Zhao, G. Q. (2019).

"Research on 3-D bio-printing molding technology of tissue engineering scaffold by nanocellulose-gelatin hydrogel composite," *BioResources* 14(4), 9244-9257. DOI: 10.15376/biores.14.4.9244-9257

Danso, E. K., Julkunen, P., and Korhonen, R. K. (2018). "Poisson's ratio of bovine meniscus determined combining unconfined and confined compression," *J. Biomech.* 77, 233-237. DOI: 10.1016/j.jbiomech.2018.07.001

Fozdar, D. Y., Soman, P., Lee, J. W., Han, L. H., and Chen, S. (2011). "Three-dimensional polymer constructs exhibiting a tunable negative Poisson's ratio," *Adv. Funct. Mater.* 21(14), 2712-2720. DOI: 10.1002/adfm.201002022

Hribar, K. C., Soman, P., Warner, J., Chung, P., and Chen, S. (2014). "Light-assisted direct-write of 3D functional biomaterials," *Lab Chip* 14(2), 268-275. DOI: 10.1039/c3lc50634g

Huang, J., Liu, W., and Tang, A. (2018). "Effects of fine-scale features on the elastic properties of zero Poisson's ratio honeycombs," *Mater. Sci. Eng. B* 236-237, 95-103. DOI: 10.1016/j.mseb.2018.11.005

Jurvelin, J. S., Arokoski, J. P. A., and Hunziker, E. B. (2000). "Topographical variation of the elastic properties of articular cartilage in the canine knee," *J. Biomech.* 33(6), 669-675. DOI: 10.1016/S0021-9290(00)00007-5

Leppiniemi, J., Lahtinen, P., Paajanen, A., Mahlberg, R., Metsa-Kortelainen, S., Pinomaa, T., Pajari, H., Vikholm-Lundin, I., Pursula, P., and Hytonen, V. P. (2017). "3D-printable bioactivated nanocellulose-alginate hydrogels," *ACS Appl. Mater. Inter.* 9(26), 21959-21970. DOI: 10.1021/acsami.7b02756

Li, H., Tan, Y. J., Leong, K. F., and Li, L. (2017). "3D bioprinting of highly thixotropic alginate/methylcellulose hydrogel with strong interface bonding," *ACS Appl. Mater. Inter.* 9(23), 20086-20097. DOI: 10.1021/acsami.7b04216

Lim, C., Shin, Y., Jung, J., Kim, J. H., Lee, S., and Kim, D.-H. (2019). "Stretchable conductive nanocomposite based on alginate hydrogel and silver nanowires for wearable electronics," *APL. Mater.* 7(3), Article ID 031502. DOI: 10.1063/1.5063657

Liu, Y. J., Cao, W. T., Ma, M. G., and Wan, P. (2017). "Ultrasensitive wearable soft strain sensors of conductive, self-healing, and elastic hydrogels with synergistic "Soft and hard" hybrid networks," *ACS Appl. Mater. Inter.* 9(30), 25559-25570. DOI: 10.1021/acsami.7b07639

Mandrycky, C., Wang, Z., Kim, K., and Kim, D. H. (2016). "3D bioprinting for engineering complex tissues," *Biotechnol. Adv.* 34(4), 422-434. DOI: 10.1016/j.biotechadv.2015.12.011

Men, Y. T., Li, X. M., Yang, N., Wang, X., and Zhang, C. Q. (2018). "Analysis of the mechanical effects of defect shape on damage evolution of articular cartilage under rolling load," *Mater. Sci. Eng. C* 92, 407-415. DOI: 10.1016/j.msec.2018.06.058

Nguyen, D., Hagg, D. A., Forsman, A., Ekholm, J., Nimkingratana, P., Brantsing, C., Kalogeropoulos, T., Zaunz, S., Concaro, S., Brittberg, M., *et al.* (2017). "Cartilage tissue engineering by the 3D bioprinting of iPS cells in a nanocellulose/alginate bioink," *Sci. Rep.* 7(1), Article Number 658. DOI: 10.1038/s41598-017-00690-y

Saito, T., Kimura, S., Nishiyama, Y., and Isogai, A. (2007). "Cellulose nanofibers prepared by TEMPO-mediated oxidation of native cellulose," *Biomacromolecules* 8(8), 2485-2491. DOI: 10.1021/bm0703970

Soman, P., Lee, J. W., Phadke, A., Varghese, S., and Chen, S. (2012). "Spatial tuning of negative and positive Poisson's ratio in a multi-layer scaffold," *Acta Biomater.* 8(7), 2587-2594. DOI: 10.1016/j.actbio.2012.03.035

Stahl, P. J., Chan, T. R., Shen, Y. I., Sun, G., Gerecht, S., and Yu, S. M. (2014). "Capillary network-like organization of endothelial cells in PEGDA scaffolds encoded with angiogenic signals *via* triple helical hybridization," *Adv. Funct. Mater.* 24(21), 3213-3225. DOI: 10.1002/adfm.201303217

Sun, C., Fang, N., Wu, D. M., and Zhang, X. (2005). "Projection micro-stereolithography using digital micro-mirror dynamic mask," *Sensor Actuat. A-Phys.* 121(1), 113-120. DOI: 10.1016/j.sna.2004.12.011

Tang, A., Li, J., Li, J., Zhao, S., Liu, W., Liu, T., Wang, J., and Liu, Y. (2019). "Nanocellulose/PEGDA aerogel scaffolds with tunable modulus prepared by stereolithography for three-dimensional cell culture," *J. Biomat. Sci.-Polym. E.* 30(10), 797-814. DOI: 10.1080/09205063.2019.1602904

Tang, A., Wang, Q., Zhao, S., and Liu, W. (2018). "Fabrication of nanocellulose/PEGDA hydrogel by 3D printing," *Rapid Prototyping J.* 24(8), 1265-1271. DOI: 10.1108/rpj-03-2016-0049

Tilleman, T. R., Tilleman, M. M., and Neumann, M. H. A. (2004). "The elastic properties of cancerous skin-Poisson's ratio and Young's modulus," *Israel Med. Assoc. J.* 6(12), 753-755.

Wang, N., Liu, W., Tang, A., Huang, J., Lin, Z., and Lei, S. (2014). "Strain isolation: A simple mechanism for understanding and detecting structures of zero Poisson's ratio," *Phys. Status Solidi B* 251(11), 2239-2246. DOI: 10.1002/pssb.201451376

Wang, Z., Abdulla, R., Parker, B., Samanipour, R., Ghosh, S., and Kim, K. (2015). "A simple and high-resolution stereolithography-based 3D bioprinting system using visible light crosslinkable bioinks," *Biofabrication* 7(4), Article ID 045009. DOI: 10.1088/1758-5090/7/4/045009

Zheng, C., Yue, Y., Gan, L., Xu, X., Mei, C., and Han, J. (2019). "Highly stretchable and self-healing strain sensors based on nanocellulose-supported graphene dispersed in electro-conductive hydrogels," *Nanomaterials* 9(7), Article Number 937. DOI: 10.3390/nano9070937

Article submitted: January 17, 2020; Peer review completed: March 14, 2020; Revised version received and accepted: March 18, 2020; Published: March 24, 2020.
DOI: 10.15376/biores.15.2.3307-3319